1	Engineered Ru on HY Zeolite Catalyst for Continuous and Selective
2	Hydrodeoxygenation of Lignin Phenolics to Cycloalkanes Under Moderate
3	Conditions
4	Adarsh Kumar ^{a,b} , Abhishek Kumar ^c , Daniel M Santosa ^c , Huamin Wang ^c , Peng Zuo ^d ,
5	Chongmin Wang ^d , Ashutosh Mittal ^b , Rafal Gieleciak ^e , Darryl P. Klein ^f , Michael J Manto ^f ,
6	Bin Yang ^{a*}
7 8 9 10 11 12 13 14 15 16 17 18 19	 ^aBioproducts, Sciences, and Engineering Laboratory, Department of Biological Systems Engineering, Washington State University, Richland, Washington, 99354, United States ^bRenewable Resources and Enabling Sciences Center, National Renewable Energy Laboratory, Golden, CO 80401, United States ^cEnergy and Environment Directorate, Pacific Northwest National Laboratory, Richland, Washington 99352, United States ^dEnvironmental Molecular Sciences Laboratory, Pacific Northwest National Laboratory, Richland, Washington 99354, United States ^eNatural Resources Canada, CanmetENERGY Devon, One Oil Patch Drive, Devon, AB, T9G 1 A8, Canada ^f Advanced Refining Technologies, LLC, Baltimore, Maryland, United States *Corresponding Author, Email: bin.yang@wsu.edu
20	
21	Abstract
22	
23	We report a continuous selective hydrodeoxygenation (HDO) process of guaiacol conversion
24	to cycloalkanes under 180 $^{\circ}\text{C/1}$ MPa, which results in improved HDO chemistry for lignin-
25	based jet fuel production. The incipient wetness impregnation method was modified to prepare
26	an HY zeolite-supported Ru catalyst with better metal dispersion and acid site uniformity,
27	which overcomes the low conversion and selectivity of previous literature. The modified
28	catalyst (Ru-HY-60-MI) was tested in a continuous fixed bed reactor, resulting in increased
29	HDO conversion of guaiacol to cycloalkanes compared to the unmodified catalyst. Pressure,
30	temperature, and weight hourly space velocity-dependent tests validate guaiacol HDO over Ru-
31	HY-60-MI catalyzed ring hydrogenation of guaiacol to 2-methoxycyclohexanol, acid-
32	catalyzed demethoxylation and dehydration to cyclohexene, and further hydrogenation of
33	cyclohexene to cyclohexane. These experiments enable exploring a continuous HDO process,

- demonstrate effectiveness for other β - β and α -O-4 lignin representatives and real lignin bio-
- oil, and pave the way towards commercialization of lignin-based jet fuel.
- 36 **Keywords:** Continuous hydrodeoxygenation, Engineered catalyst, Cycloalkanes, Lignin bio-

As the largest source of renewable aromatics in nature, lignin could hold the answer to

oil, Moderate conditions, Sustainable biorefinery

1. Introduction

38

39

40

41

42

43

44

45

46

47

48

49

50

51

52

53

54

55

56

57

58

achieving a lignin-based jet fuel pathway, which allows Sustainable Aviation Fuel (SAF) to have fuel system compatibility at higher blend ratios [1-5]. The lignin depolymerized product from liquefaction (oxidative, reductive, and inert) and pyrolysis possess high concentrations of phenolics, such as phenols, guaiacols, and syringols [6, 7]. The carbon number of these phenolics is in the jet/gasoline range. However, their direct usability is restricted due to the presence of oxygen content [8]. Therefore, these oils must undergo hydrodeoxygenation to increase the C/H ratio and reduce the oxygen content to meet the fuel quality standards. Guaiacol having the most representative functionalities (i.e., hydroxyl (-OH) and methoxy (-OCH₃) groups), has been frequently used as a surrogate to identify the efficient routes for lignin processing in fuel applications [9, 10]. Notably, HDO studies of guaiacol have been carried out in batch process [11-15]. However, developing industrially viable HDO processes requires a deeper understanding of HDO chemistry in the continuous process [16]. Although continuous catalytic HDO processes look promising, they are still in the development phase. Several zeolites (HY, H\beta, HZSM-5), TiO₂, SiO₂, Al₂O₃, and carbon catalysts have been investigated due to their suitable surface area, pore channels, and acid sites (Table 1). TiO₂, SiO₂, and Al₂O₃ show lower deoxygenation activity compared to zeolites, presumably because of the absence of Brønsted acid sites [17-19]. Zeolites exhibit a balance between acid sites, pore size, thermal stability, and surface area for shape selective HDO. Table 1 reveals a continuous flow system requires a high reaction

temperature (300 - 450 °C) and high hydrogen pressure (3-7 MPa) to produce ring-saturated products without oxygen. Moreover, most studies used organic solvents (i.e., toluene, n-hexadecane, etc.) as diluting agents with guaiacol. However, the dilution step is associated with the higher cost of the process and limits its scalability [20, 21].

Table 1: The survey of the reaction conditions and performance for the continuous catalytic HDO process of guaiacol in both atmospheric and high hydrogen pressure.

				Reac	tion cor	ditions					
Year	Guaiacol conc., %	Solvent	Catalyst	T, °C	P, MP a	W/F, h	Conversio n,%	Cyclic alkan es	Aromatic s	Gas	_ Ref
Atmosph	neric hydroge	n pressure									
2011	100	-	Ni ₂ P/SiO ₂	300	0.1	0.71	80	0	60	NA	[22]
2013	100	-	Pd-Fe/C	450	0.1	0.75	98	0	87	11	[23]
2013	100	-	Ni ₂ P/SiO ₂	300	0.1	1.5	99.5	0	71.9	5.7	[24]
2013	100	-	Fe/SiO ₂	400	0.1	7.5	100	0	75	17	[25]
2014	100	-	Pt/C	300	0.1	0.3	88	0	0	22	[26]
2016	100	-	Co/Al-MCM-41	400	0.1	1.67	99.5	0	34.4	29.7	[27]
2016	100	-	Fe/Ni/Hbeta	400	0.1	4.0	100	5.59	6.11	1.79	[28]
2016	100	-	Ni@Pd SD	450	0.1	2.4	83	0	52	NA	[24]
2018	100	-	PdRe/C	300	0.1	1	85	18	40	5	[29]
2022	100	-	Pd-Fe/AL- MCM-11	400	0.1	1.67	100	45	5	24.3	[27]
High hyd	lrogen pressu	ire									
2012	3 wt%	-	Pt/MZ-5	200	4.0	2	100	92	0	NA	[30]
2014	1 wt%	Tridecane	Ni ₂ P/SiO ₂	300	0.8	0.5	100	91	8	NA	[31]
2014	3 wt%	Dodecane	Pt/TiO ₂ ,	300	7.1	0.04	88.1	89	0	NA	[32]
			NiMo/Al ₂ O ₃				94.3	88.6			
2014	0.4 mol%	-	Pt/MgO	250	6.9	0.27	62.9	25	0	10	[20]
2015	5 wt%	Octanol	Pt/MFI	200	10	2.7	100	97	0	NA	[33]
2016	10 wt%	Dodecane	Pt-Mo/TiO ₂	285	4	2.85	95	73.4	0	5.2	[32]
2016	100%	-	Au ₅₅ Rh ₄₅ /TiO ₂	280	4	0.33	94	75	0	NA	[34]
2016	3 wt%	-	CoMoS/CCA	260	3	2.38	92	11	31.5	NA	[21]
2017	100%	-	Ni ₅ Fe ₁ /CNT	300	3	0.33	100	99.8	0	NA	[35]

2017	3 wt%	Dodecane	Pd/TiO ₂ (A)	280	2	-	100	70	10	NA	[36]
2019	50 wt%	Dodecane	Rh/HY	250	4	1	100	71.3	0	NA	[8]
2019	5 wt%	Dodecane	Pt/H-ZSM5	260	3	3.33	100	100	0	NA	[37]
2019	100%	-	NiCNT+ WxC@CS	300	3	1.64	100	91	5	NA	[38]
2020	100%	-	Ni/BEA-IDP	230	4	0.005	10.4	52.8	0	NA	[39]
2020	2 wt%	Dodecane	10Ni- 20Mo/Al ₂ O ₃ - TiO ₂	300	2	1.71	100	97	3	NA	[40]
2021	100%	-	Ion Exchanged Ru/BEA	200	4	0.19	17.7	14.6	0	NA	[41]
2023	100%	-	Ru-HY-60-MI	180	1	1	100	87	0	NA	This
											study

Under moderate HDO conditions, the guaiacol conversion encounters several challenges, including low conversion rates, diminished hydrodeoxygenation product yields, and catalytic site poisoning [8]. Developing durable, active, selective, and regenerable bifunctional catalysts for use at moderate reaction conditions is critically important to forming saturated hydrocarbons with maximum carbon retention [33]. Ru-based zeolites are cheaper and more selective compared to Pt and Pd-based zeolites [42, 43]. Traditional incipient wetness impregnation is widely embraced for metal impregnation due to its technical simplicity and minimal waste generation. However, this methodology leads to significant metal aggregation and low metal dispersion on the external surface of supports, which resulted in low activity [41, 44]. Therefore, a high metal loading is needed to maintain the catalyst activity, and it increases the catalyst cost [45].

To improve the metal dispersion and metal content on the zeolite surface, herein, traditional incipient wetness impregnation has been modified to prepare HY zeolite-supported Ru catalyst. As we identified HY best support for lignin HDO among all zeolites in our previous studies [3, 46-48]. The difference in catalyst properties and performance results is demonstrated over modified and traditional impregnated catalysts. Moreover, the activity of the modified catalyst is evaluated for a broader range of reaction parameters, such as feed flow,

temperature, and pressure to explore the reaction mechanisms. This understanding would further extend the efficient continuous HDO process of other lignin representatives (β - β and α -O-4) and extend to real lignin bio-oil. The findings of this research significantly contribute to advancing knowledge of HDO chemistry in moderate conditions, and such advancements can unlock new potentials for continuous lignin HDO to sustainable aviation fuel.

2. Materials and methods

2.1 Chemicals

CBV 400 is a commercial product purchased from Zeolyst International Inc. (Conshohocken, PA, US). RuCl₃.H₂O and Guaiacol were procured from Sigma-Aldrich. Ethyl acetate, methanol and citric acid were purchased from Alfa Aesar. National Renewable Energy Laboratory supplied the lignin black liquor and lignin was purified according to previously published works of our group [47, 49].

2.2 Catalysts synthesis methodology

60% HY zeolite was synthesized using 40% inert material (clay) to bind HY Zeolite (CBV 400) in the form of extrudates. The extrudates were subsequently utilized for ruthenium impregnation. An aqueous RuCl₃ solution was made using 0.104 g RuCl₃ per mL of water. The appropriate amount of RuCl₃ aqueous solution was used to meet the 2 wt% Ru loading, and extra water was used to saturate the pores of the support extrudates (~0.77 mL g⁻¹). The resultant catalyst is named Ru-HY-60-I. Furthermore, a 100% HY zeolite-based catalyst (Ru-HY-100-I) was prepared following the same impregnation method as previously stated. A physical mixture catalyst (PM) was also prepared with 60% Ru-HY-100-I and 40% inert material.

The modified impregnation method was also employed to synthesize a ruthenium zeolite catalyst (Ru-HY-60-MI), where 0.10 g citric acid was added per mL water besides ruthenium chloride, while the remaining steps were the same without any change.

All catalysts were dried at 100 °C after preparation and subsequently calcined at 500 °C under an air atmosphere for 30 min. All catalysts were sieved in mesh size (60-80) for the experiment, and in the case of modified catalysts, thorough washing was performed with hot water to eliminate any residual citric acid prior to sieving.

2.3 Catalyst characterization methodologies

X-ray diffraction (XRD) was used to identify the crystallinity and structure of the catalysts. XRD patterns were recorded using a MiniFlex II diffractometer in the 5-85° range with 0.02° step interval and a scan speed of 4° per minute. Cu Kα with a wavelength of 1.5418 Å was used as a source of radiation. Thermogravimetric analysis (TGA) was performed in NETZSCH STA 449F1 instrument using 100 mL min⁻¹ air flow. Weight loss was measured in the temperature range of 25 to 800 °C with heating rate of 10°C min⁻¹.

Surface area, pore size, and pore volume were evaluated using N₂-physisorption. Normally, Ru-HY-60-MI was dried at 550 °C for 3 h in an oven to remove volatiles. Dried Ru-HY-60-MI was loaded into a glass tube and weighed. The tube containing Ru-HY-60-MI was then placed in the Micromeritics Smart VacPrep for pre-treatment at 175 °C. After pre-treatment, the tube was reweighed and loaded onto Micromeritics Tristar 2 Plus nitrogen porosimeter. A 60-point method where relative pressure readings were taken in a liquid nitrogen bath is conducted over 15 h. The surface area was calculated using the Brunauer-Emmett-Teller (BET) method.

Inductively coupled plasma atomic emission spectroscopy (ICP-AES) was used to identify the metal compositions. Typically, Ru-HY-60-MI surface was cleaned in an oven at 550 °C for 5 h. The cooled Ru-HY-60-MI was finely ground using mortar and pestle, and a

quantitative portion of ground Ru-HY-60-MI was dissolved in an acid matrix. The resulting mixture was heated to ensure the complete dissolution of Ru-HY-60-MI, followed by cooling and dilution. The diluted sample was analyzed using Agilent 5110 ICP-AES. The analytical procedure involved utilizing both high and low standard concentrations for the element's identification, along with an analysis of quality control measures to ensure proper calibration. Additionally, a blank sample was run to establish a baseline.

H₂ temperature-programmed reduction (H₂-TPR) and chemisorption of catalyst were carried out on Micromeritics, AutoChem II 2920. In-built thermal conductivity detector (TCD) recorded the signals during analysis. The catalyst samples were pre-treated at 300 °C for 1 h under an argon/helium atmosphere before undergoing additional treatment. TPR was recorded with 10 vol% hydrogen in argon within the temperature range of 50-900 °C at 10 °C min⁻¹ heating rate. 10 vol% carbon monoxide in helium 10 vol% used for chemisorption in pulse mode at 50 °C to identify the metal dispersion.

The acidity characteristics of Ru-HY-60-MI were assessed through temperature-programmed desorption (TPD) using NH₃ as a probe molecule on a ChemiSorb 2720 equipped with TCD. Ru-HY-60-MI surface was cleaned at 200 °C under 50 mL min⁻¹ flow of N₂ for 1 h. Cleaned Ru-HY-60-MI was saturated with 5 mL min⁻¹ of pure ammonia at 25 °C for 30 min. Subsequently, the saturated sample was gradually heated at a ramping rate of 10 °C min⁻¹ to 700 °C, under an argon flow of 30 mL min⁻¹. The TCD signals were continuously recorded throughout the heating process to obtain the TPD pattern.

Morphology and spatial distribution of elements in the particle were analyzed using scanning/transmission electron microscopy (S/TEM), which was carried out on Titan 80-300 with probe forming lens aberration corrector (Thermo Fisher Scientific, Inc.) at an operating voltage of 300 kV. STEM- energy-dispersive X-ray spectroscopy (STEM-EDS) measurements were performed inside the TEM using an X-Max silicon solid state detector (Oxford

Instruments, PLC.) for the compositional analysis. The sample powders were dispersed on a lacey carbon formvar Au grid for the STEM studies.

2.4 Catalytic reactions

158

159

160

161

162

163

164

165

166

167

168

169

170

171

172

173

174

175

176

177

178

179

180

181

182

HDO reactions were performed in an in-house customized single-pass trickle bed bench-scale hydrotreater with continuous down-flow at Pacific Northwest National Laboratory (Figure S1). The detailed description of reactor is given in the previous publication [50]. 5 g catalyst was packed in 26 inches long hastelloy C tubing with a 0.75 inches internal diameter. The packed reactor was tested for leaking nitrogen at desired reaction pressure. Mass flow controller was used to feed H₂ with a flow of 100 mL min⁻¹ for in-situ reduction of catalyst at reaction temperature before the experiment and same H2 flow was used all through experiment. The temperature of the reactor was maintained using dual stage furnace having control panels. A back-pressure regulator was used to maintain the pressure of the experiment. After catalyst reduction and retaining pressure, a high pressure ISCO pump was used to deliver the reactant (lignin in aqueous base) in the reactor. Formed liquid products in experiments were condensed in pressurized gas-liquid separator (downside of reactor) with cooled traps. Out flow of gases was measured using the digital DryCal gas meter after passing through the back-pressure regulator then off gas directed to an online Inficon Micro-GC 3000 four-channel micro-GC instrument for compositional analysis. The liquid product was collected over the entire experimental duration at 1 h time interval.

2.5 Product analysis

Qualitative and quantitative identifications of the organic compounds were carried out using a combination of analytical techniques. In this study, we used a combination of analytical techniques including two-dimensional gas chromatography coupled with a flame ionization detector (GC×GC-FID), GC×GC with time-of-flight mass spectrometry (TOF-MS), and GC-MS to perform the qualitative and quantitative identifications of the organic compounds. The

mass of gaseous products calculated according to data recorded on online Inficon Micro-GC 3000 four-channel micro-GC instrument. Mass of solid products calaculated weight loss during calcination of spent catalyst. All results are reported with $\pm 2\%$ error. A detailed description is provided in the supplementary information section for a comprehensive overview of the instrumentation and methodologies used. The conversion, selectivity, and yield of products were calculated according to our previous publications [51, 52]. The conversion was calculated on weight of feed and products. Mass balance was calculated according to weight of total products.

191 Conversion, wt% =
$$|1 - \frac{\text{weight of the reactant comming out of the reactor}}{\text{weight of the reactant going inside the reactor}}| x 100$$
 (1)

193 Liquid yield, wt% =
$$\left| \frac{\text{weight of all material coming out reactor}}{\text{weight of material feeding into reactor}} \right| x100$$
 (2)

195 Selectivity, wt% =
$$\left| \frac{\text{weight of organic product A}}{\text{weight of all organic liquid products}} \right| X100$$
 (3)

3. Results and Discussion

183

184

185

186

187

188

189

190

192

194

196

197

198

199

200

201

202

203

204

205

206

207

208

209

3.1 Catalyst characteristics

The difference in textural properties of different Ru-based catalysts was investigated by using N₂ porosimetry (Table 2). Pore diameters (PD) calculated by Barrett–Joyner–Halenda (BJH) and pore volume data show that these are higher for engineered extrudates than parent HY. BET surface area of Ru-HY-60-I is smaller than that of the parent extrudates owing to large Ru particles on the surface. Ru-HY-100-I exhibits the same phenomenon in surface area observation (Table 2, entries 1 and 3). However, the BET surface area for Ru-HY-60-MI remains nearly unchanged when compared to parent extrudates. This fact could be attributed to the presence of highly dispersed small Ru nanoparticles in Ru-HY-60-MI. While the pore size data suggest a decrease in pore size for Ru-HY-60-MI (0.04 nm), is somewhat higher than Ru-HY-60-I (0.02 nm), attributed to some small ruthenium nanoparticles within pores and validated with low pore volume [53]. A drastic change in textural properties for S-Ru-HY-60MI (spent catalyst after experiment) was observed due to coke deposition on the surface and in the pores of catalysts (TGA and TEM images in Figure S2).

Table 2: Textural parameters of the catalyst samples.

Catalyst	Surface Area, m ² g ⁻¹	Average pore diameter, nm	Pore volume, cm ³ g ⁻¹	Ru content ^a , wt%	Average Ru particle size ^b , nm	Metal dispersion ^c		
HY	724	0.73±0.2	0.40		-	-		
HY-60-Extrudate	468	0.86 ± 0.2	0.46	-	-	-		
Ru-HY-100-I	631	0.72 ± 0.2	0.33	2.02	-	-		
PM	462	0.80 ± 0.2	0.46	1.60	-	-		
Ru-HY-60-I	443	0.84 ± 0.2	0.45	1.95	3.4±0.2	8.5		
Ru-HY-60-MI	467	0.82 ± 0.2	0.43	2.07	2.9±0.05	16.2		
S-Ru-HY-60-MI	59	0.65 ± 0.2	0.13	1.80*	-			

a ICP-AES

S - Spent catalyst

XRD of catalysts revealed diffraction peaks positions identical to HY zeolites (6.1, 10.3, 15.9, and 23.9°) in all corresponding Ru functionalized materials (Figure 1a), which indicates that the crystallinity of HY zeolite remained intact after catalyst engineering as well as Ru impregnation [54]. The intense signature peaks in Ru-HY-100-I indicate a high amount of HY zeolite and no inert material.

NH₃-TPD profiles of all catalysts are given in Figure 1b and Figure S3. Two peaks in catalysts were assigned to the weak acidic sites (mainly surface hydroxyl sites, below 275 °C) and medium acid sites (300-500 °C), respectively (Figure S3). Ru-HY-60-MI and Ru-HY-60-I have stronger medium acidic sites than Ru-HY-100-I and PM [51], as seen from the notable shift in NH₃ desorption peak at temperatures greater than 300 °C. The highest acid site density of Ru-HY-100-I can be seen in Figure 1b, as expected, compared to diluted zeolite-based catalysts (Ru-HY-60-MI, Ru-HY-60-I, and PM). The presence of small ruthenium nanoparticles in zeolite pores leads to a slight decrease in acid site density in Ru-HY-60-MI compared to Ru-HY-60-I [41, 55] (Figure 1b). In summary, Ru-HY-60-MI has the lowest overall acid site density but stronger strength of medium acidic sites.

^b Calculated using TEM images

^c CO Chemisorption

^{*} ICP-AES after subtraction of carbon content

TPR profiles of the Ru-HY-60-MI and Ru-HY-60-I catalysts (Figure 1c) exhibit two reduction zones ≤250 °C and ≥ 250 °C, which indicate two types of RuO₂ domains with different intensities of interaction with support. An intense TPR peak (≤250 °C) of Ru-HY-60-MI starts at a lower temperature in a doublet form compared to Ru-HY-60-I. It ascribes the different locations of the highly dispersed RuOx species in the zeolite structure [56, 57] and consistent with CO-chemisorption data (Table 2). The addition of acetic acid in modified impregnation method generates C₂H₃O₂⁻ ions, and C₂H₃O₂⁻ ions resulted in Ru nanoparticles with a narrow size distribution because of its potent ability to stabilize the primary Ru nanoparticles [58, 59]. Furthermore, the intensity of both TPR peaks for Ru-HY-60-MI is significantly high. This suggests Ru-HY-60-MI is adsorbing more hydrogen because of the large number of Ru particles on its surface. The TEM observation can support well TPR profiles of both catalysts to validate particle number and its size presence. TEM analysis of Ru-HY-60-MI and Ru-HY-60-I show notable differences in Ru size (Figure 2 and Table 2). In particular, a significant number of smaller Ru particles with a diameter of ≤2.5 nm is present in Ru-HY-60-MI (Figures 2c, 2g and S4). This observation is further supported by the elemental mapping (Figures 2d and 2h) and average particle size calculations (Table 2) of Ru in both catalysts. Specifically, the Ru mapping in Ru-HY-60-MI exhibits a homogeneous distribution, while in Ru-HY-60-I, some large Ru clusters are visible. These observations indicate that the modified impregnation synthesis method is successful in integrating Ru nanoparticles onto the support surface with high efficiency. Moreover, despite the modification of zeolite composition, no change in zeolite structure is observed, as confirmed by selected-area electron diffraction (SAED) patterns (Figure S4) for both samples, which is clearly observed by the highly crystalline state of these as of HY zeolite. Lattice fringes are captured from Ru by STEM, as illustrated in Figures 2c and 2g. The derived interplanar spacing suggests that both cubic and hexagonal Ru are possible to be formed in Ru-HY-60-MI (measured: 0.2 nm; cubic: $d_{111} = 2.19 \text{ Å}$, $d_{200} = 1.90 \text{ Å}$;

229

230

231

232

233

234

235

236

237

238

239

240

241

242

243

244

245

246

247

248

249

250

251

252

hexagonal: $d_{002} = 2.14$ Å, $d_{1-11} = 2.06$ Å), whereas hexagonal Ru is more likely to be formed in Ru-HY-60-I (measured: 0.3 nm; hexagonal: $d_{100} = 2.71$ Å) [60, 61].

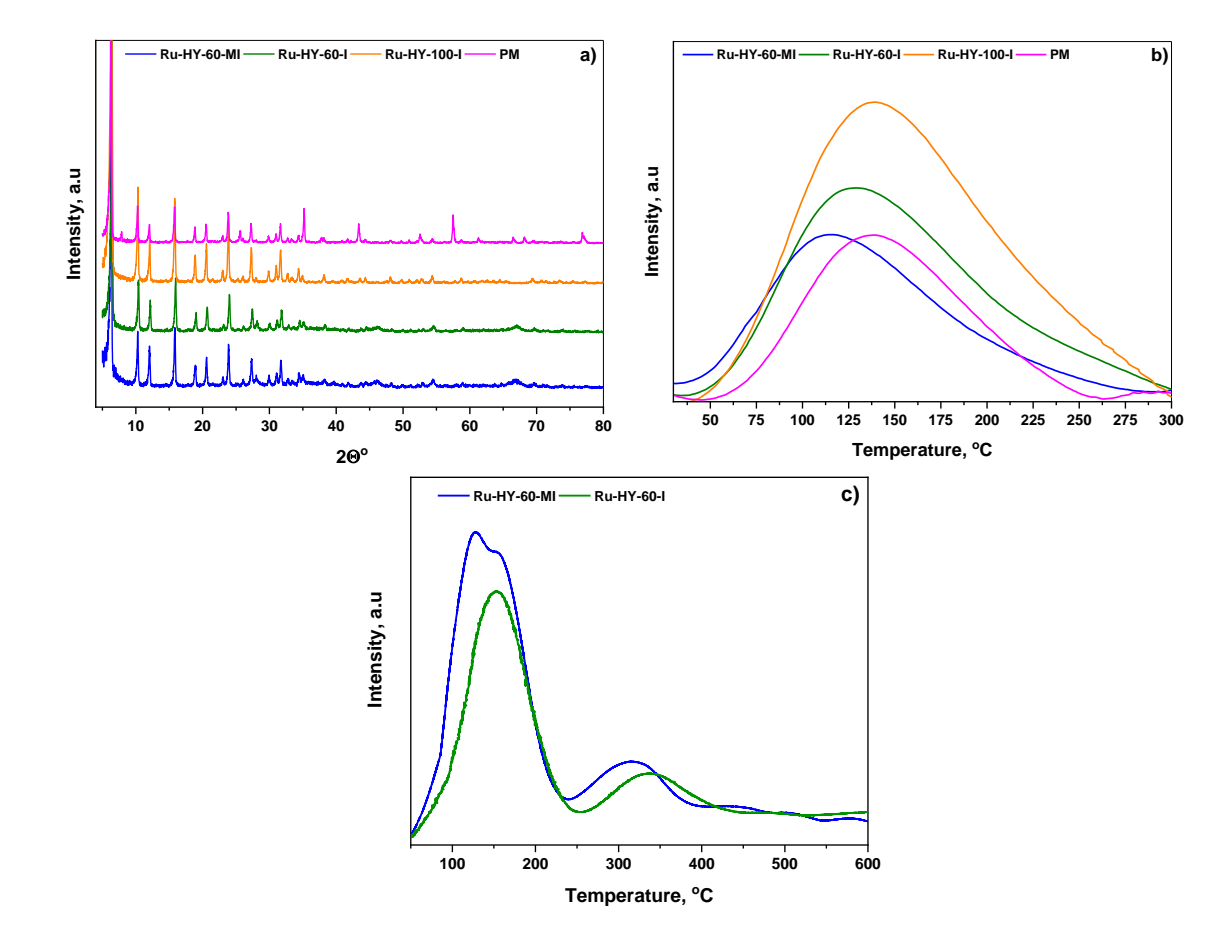


Figure 1: a) XRD pattern; b) NH_3 -TPD profile and c) TPR profile of catalysts.

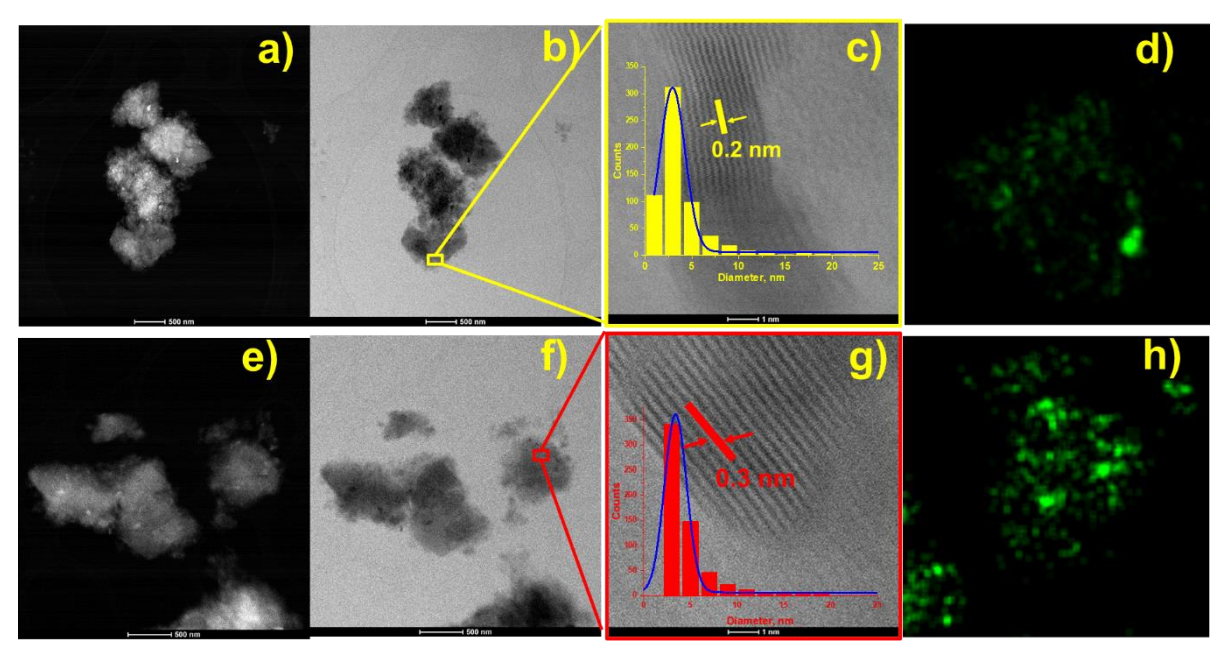


Figure 2: Structural and chemical analysis of Ru-HY-60-MI (the top row) and Ru-HY-60-I (the bottom row) by TEM. (a,e) STEM- high-angle annular dark field (STEM-HAADF) and (b,f) STEM-

bright filed (STEM-BF) images of prepared catalysts with (d,h) Ru STEM-EDS mapping; (c,g) STEM-BF images along with measured interplanar spacing and metal particles size distributions.

3.2 Guaiacol hydrodeoxygenation

3.2.1 Catalyst evaluation

Designing a highly efficient engineered bifunctional catalyst for the HDO under moderate reaction conditions poses a significant challenge. This difficulty arises from the competing reactions of ring saturation and C–O hydrogenolysis, which hinder the production of ring-saturated hydrocarbons. HY alone as the catalyst is insufficiently active for saturated hydrocarbon production. However, incorporating a small quantity of Ru is excellently capable for H₂ activation and effective facilitation of activated H₂ for the HDO process [62, 63]. Figure 3 depicts the time-on-stream (TOS) results of Ru-based HY catalysts evaluated in this study for guaiacol HDO. A wide range of conversions was obtained for the complete screening of catalysts. The results indicated that the acid site amount and its distribution had a considerable impact on the HDO of guaiacol. Moreover, the integration of active metal sites with acid sites was crucial for HDO activity and product selectivity.

Ru-HY-100-I showed complete conversion and selectivity for cycloalkanes within a 2 h reaction time. Nonetheless, a minor decline in both conversion and cycloalkane content became evident after 3 hours, subsequently leading to the rapid deactivation of Ru-HY-100-I. This deactivation can be attributed to the dense and high number of acidic sites in the HY-zeolite structure [47]. These acidic sites cause extensive cracking reactions, resulting in reduced liquid product yield and high content of gaseous products (Table S1) [51, 52, 64].

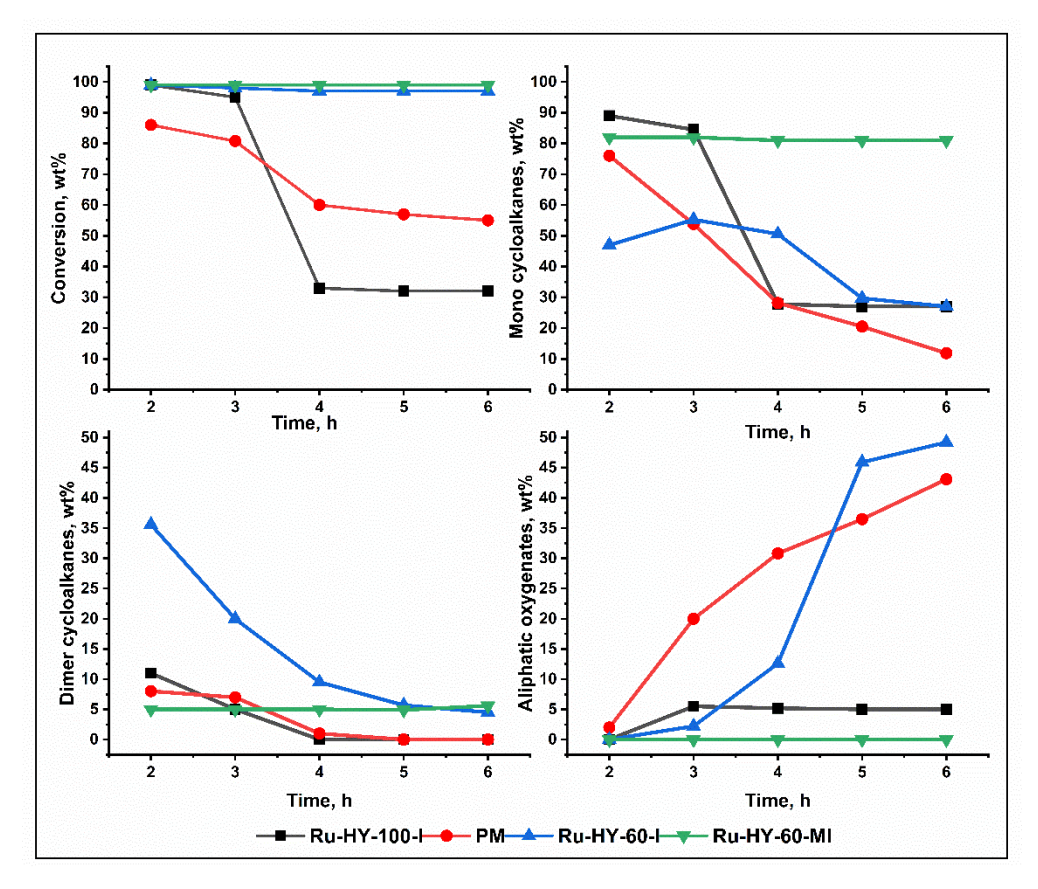


Figure 3: Guaiacol conversion and product yields with different catalysts as a function of time on stream. Reaction conditions: Pressure - 1 MPa, Temperature - 180 °C, WHSV - 1 h^{-1} All results are with $\pm 2\%$ error.

Extensive cracking reflected in rapid coke formation and deactivation of Ru-HY-100-I (Figure 4a). Moreover, a drastic decrease in characteristic zeolite peak near 6.3° in XRD of spent Ru-HY-100-I (Figure 4b) further validates the highest coke deposition on the Ru-HY-100-I surface, which covered the available active sites for HDO. To change the acid-site accessibility of guaiacol molecules, the acid site density and their numbers were tuned using an inert diluting agent to manage the strength of acidic sites. As strong acid sites promote cyclohexanol deoxygenation, and hence the combination of proper number of acid sites and Ru nanoparticles are retained and can work best for HDO [51]. We think that inert material only reduces the acidity and does not change nature/type of the acidity. A physical mixture of 60% Ru-HY-100-I and 40% inert material (60% HY zeolite composition) exhibited a maximum 86% conversion and 84% yield of cycloalkanes. In contrast to low activity, the deactivation rate of the catalyst was slow compared to 100% HY zeolite. The low and decreasing activity

of PM over time reveals the importance of the balanced number of acidic sites (Figure 3). However, the presence of aliphatic oxygenates throughout the TOS suggests lack of proximity between the Ru and acid sites.

Ru-HY-60-MI and Ru-HY-60-I demonstrated almost complete conversion over the whole TOS. Alkane oxygenates appearance for Ru-HY-60-I define the Ru particle size and its dispersion-dependent activity. Ruthenium particles are bigger and non-homogeneously distributed with low metal dispersion in Ru-HY-60-I [65] (Figure 2 and Table 2). The large particles in Ru-HY-60-I demonstrated a high reaction rate of hydrogenation vs. deoxygenation of reacting molecules and form a reasonable amount (≈5 wt%) of alkane oxygenates [66]. The hydrogenation cum deoxygenation activity to produce cyclic alkanes was enhanced by the small Ru nanoparticles in Ru-HY-60-MI [66, 67].

Initially in TOS, a significant yield of dimers reveals the role of bare acidic sites and largest pores (among all catalysts) for the promotion of the C-C coupling reaction. These acid sites were poisoned over time for deoxygenation [6, 50] (Figure 4). A remarkable change in the product profile occurred with Ru-HY-60-MI. Complete guaiacol conversion into cycloalkanes is achieved over the entire TOS. This unique efficacy of Ru-HY-60-MI is due to highly dispersed Ru nanoparticles as seen in both Figure 2 and Table 2, where metal dispersion increased from 8.5 to 16.2 in CO chemisorption. Ru dispersion facilitates the formation of numerous small-sized ruthenium nanoparticles on the catalyst surface and within the pores. Besides this, dispersed and stabilized Ru nanoparticles form strong metal-support interaction (Figure S3) [68]. Particle-size-dependent adsorption energies of reactant molecules play a vital role in HDO reactions because of their inherent high hydrogenation cum oxophillic nature [69, 70]. The homogeneous distribution of Ru particles creates proximity with acidic sites (Figure 1b). Close proximity simplifies the spillover of guaiacol and intermediates (alkane oxygenates) to and from acid sites at the perimeter of active Ru nanoparticles [71, 72]. This phenomenon

facilitates the excellent HDO efficiency. Moreover, Ru nanoparticles within the pores of Ru-HY-60-MI can promote the HDO reaction due to passage of guaiacol molecules from the catalyst pores during the experiment [73]. In summary, product composition analysis indicates that the HDO of guaiacol is sensitive to the metal structure, acidity and their configuration.

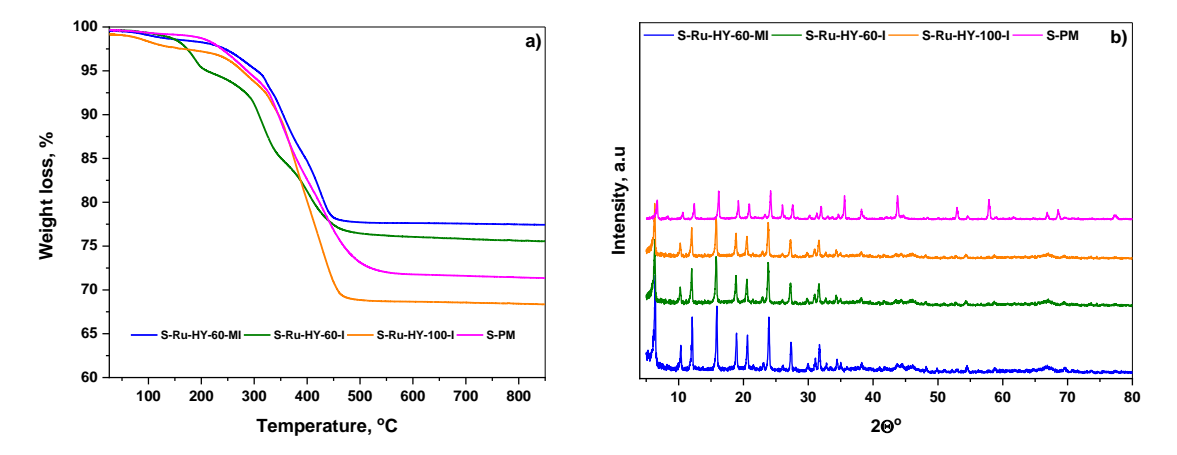


Figure 4: a) Thermogravimetric analysis; and b) XRD of spent catalysts after the HDO reaction.

3.2.2 Effect of reaction conditions

The results presented in the previous section suggest that the detailed catalytic evaluation of Ru-HY-60-MI for HDO is necessary to obtain more insightful information about activity and reaction paths. With this objective in mind, the impact of varied reaction parameters, including pressure, temperature, and WHSV were investigated for guaiacol HDO over the Ru-HY-60-MI. Ring hydrogenation was the dominant path at atmospheric pressure, suggesting the high hydrogenation ability of highly dispersed ruthenium nanoparticles. Notably, under 0.5 MPa, the prominent formation of cyclohexanol indicated that demethoxylation became a subsequent step, with its occurrence increasing as pressure rise (Table 3 and Scheme 1). The presence of 6.1% cyclohexanol. However, the product distribution drastically changed at 1 MPa, and fully deoxygenated products were identified with >99.9% guaiacol conversion. H₂ pressure directly affects the availability of hydrogen in the reaction

system, which is a driving force for overall kinetics and affects the reaction pathways [74]. Cyclohexane cracking products are thermodynamically feasible due to the presence of zeolite in the catalyst. The involvement of the cyclohexyl cation provides a reasonable pathway for the formation of dimers due to the well-known mechanism of electrophilic aromatic substitution [75, 76]. The absence or limited presence of dimers would suggest a rapid hydrogenation of the cyclohexyl cations. However, the comprehensive analysis of the reaction products reveals the appearance of hydrogenated dimers (HD), specifically methyl cyclopentyl cyclohexyl, and 1,1'-bicyclohexyl (Table 3). The presence of 1,1'-bicyclohexyl has been documented in only a limited number of literature sources [11, 77], and no comprehensive reports on the detailed reaction pathways involving this compound have been published thus far (Scheme 1). A quantitative analysis confirms the presence of these compounds in a similar ratio to their monomer content, thereby providing further evidence for the formation of methylcyclopentane. An increase in the abundance of cracking products coupled with a slight decrease in dimer concentration (Table 3) with pressure, suggests a shift in the overall reaction paths and product distribution under varied reaction conditions. Moreover, it is likely that hydrogen favors the hydroconversion of produced cyclohexane by enhancing isomerization, bimolecular and monomolecular routes, and limiting chain reactions [78]. This phenomenon further assisted the critical role of hydrogen pressure in guaiacol HDO, and it can lead to different reaction paths at different pressures (Scheme 1).

346

347

348

349

350

351

352

353

354

355

356

357

358

359

360

361

362

363

364

365

Table 3: Impact of reaction parameters on product yield and product distribution for guaiacol conversion over Ru-HY-60-MI catalyst.

	ction neter	C, wt%	Liquid yield, wt%	PEN	HEX	МСВ	MCP	СНА	MC HA	СНО	MC HO	MCPCHL	BCHL
				^^	. ^~		\bigcirc	\bigcirc	\Diamond	oH	Ů ^H	7	
Press.	1	4.8	97.4	0	0	0	0	0	0	0	4.8	0	0
MPa	0.5	67.5	93.1	0	0	2.9	0	4.7	0	19.8	29	0	1.2
	1.0	>99.9	88.6	1.3	0.8	3.5	3.3	83.2	0.5	0	0	0.5	4.5
	1.5	>99.9	87.0	1.5	1.2	3.5	6.8	80.8	1.0	0	0	0.4	3.0
Tem.	170	>99	93.0	0	0	0	0	43.4	0	15.6	40.5	0	0.5
°C	180	>99.9	88.6	1.3	0.8	3.5	3.3	83.2	0.5	0	0	0.9	4.5
	190	>99.9	86.0	1.4	0.9	3.6	6.0	81.0	1.0	0	0	0.5	4.5

	200	>99.9	83.2	2.5	1.3	3.8	6.4	77.4	1.0	0	0	0.6	5.0
	210	>99.9	65.8	2.5	1.5	4.3	6.2	76.6	1.4	0	0	0.5	4.5
	250	>99.9	54.5	3.7	2.5	6.0	7.6	70.2	3.0	0	0	0.4	1.7
WHSV,	0.5	>99.9	69.0	1.7	2.3	3.2	0	90.0	0	0	0	0	0
h⁻¹	0.75	>99.9	83.4	1.2	0.9	4.0	7.0	81.7	0.9	0	0	1.5	8.0
	1	>99.9	88.6	1.3	0.8	3.5	3.3	83.2	0.5	0	0	0.5	4.5
	1.25	>99.9	88.4	0	0	3.7	2.6	84.9	0	0	0	0.9	4.1
	1.5	>99.9	88.7	0	0	1.6	1.2	77.3	0	5.1	9.6	0.3	1.0
	2	81.8	91.9	0	0	0	0	10.4	0	11.4	55.4	0	0.8

General reaction conditions: Pressure - 1 MPa, Temperature - 180 °C, WHSV - 1 h⁻¹. Change in pressure, temperature and WHSV is mentioned in the reaction parameter column. Except mentioned change, all conditions are same

Conversion, yield and product selectivities are reported in wt%

C-Conversion, PEN-Pentane, HEX-Hexane, MCB-Methylcyclobutane, MCP-Methylcyclopentane, CHA-Cyclohexane, MCHA-Methylcyclohexane, CHO-Cyclohexanol, MCHO-1-Methylcyclohexanol, MCPCHL- Methyl cyclopentyl cyclohexyl, BCHL-1,1'-Bicyclohexyl

All results are with ±2% error

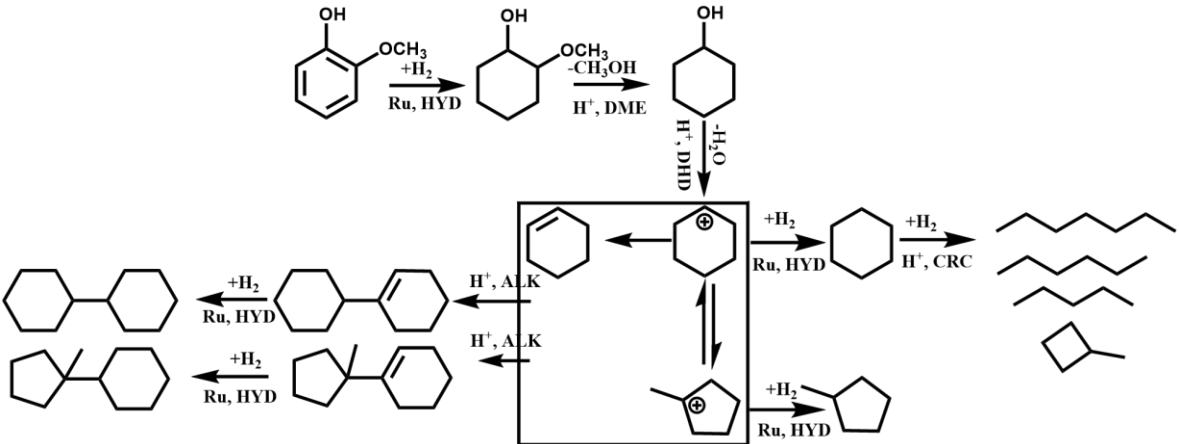
The carbon balance is in a proportional relationship with liquid yield when there is only aliphatic in the products.

Reaction temperature investigation suggests that Ru-HY-60-MI exhibits excellent reactivity for complete HDO (Table 3) of pure guaiacol at a significantly low temperature (180 °C) compared to data reported in the literature (200-300 °C), even with a low concentration of guaiacol (Table 1). Complete hydrogenated but not deoxygenated products were obtained below 180 °C. An increase in temperature influences the yield of products and their selectiveness. Low product yield and HD content with high amounts of MCB and MCP (Table 3) reflected the promotion of cyclohexane cracking at high temperatures [79]. Similarly, the high amount of methylcyclohexane shows that methyl transfer is a temperature dependent reaction.

Impact of guaiacol molecules availability in the reaction system vs. active sites was examined by variation in the WHSV. The absence of HD at a WHSV of 0.5 h⁻¹ points low availability of reacting molecules for dimer formation. However, the highest amount of HD at 0.75 h⁻¹ reveals that molecules are available in significant amounts and have reaction time enough for dimer formation. The subsequent decrease in HD content and a further increase in HD with WHSV advise that not only the long reaction time but the high amount of guaiacol molecules also promotes the dimer formation [51, 79]. The presence of aliphatic oxygenates in the product at 1.5 h⁻¹ WHSV (Table 3 and Scheme 1) suggests that the available acidic sites are insufficient for their complete deoxygenation within the given reaction time frame. A

further increase of WSHV to 2 h⁻¹ reduces conversion, proposing neither acidic nor metal sites are abundant compared to the available guaiacol molecules for HDO. An in-depth analysis of the product obtained at 2 h⁻¹ revealed the presence of guaiacol-cyclohexane dimers. This finding suggests the occurrence of a reaction between the formed cyclohexane cation and electron-rich guaiacol molecule and the subsequent HDO of this guaiacol molecule.

Pressure, temperature, and WHSV dependent results further validate guaiacol HDO over Ru-HY-60-MI proceeds via a series of steps. Initially, metal-catalyzed ring hydrogenation of guaiacol leads to 2-methoxycyclohexanol formation, followed by acid-catalyzed demethoxylation and dehydration to cyclohexene and subsequent metal-catalyzed hydrogenation of cyclohexene to cyclohexane (Scheme 1). This observation provides valuable insights into the interplay between pressure, temperature, and WHSV on the HDO process, highlighting the complex nature of the reaction dynamics.



Scheme 1: Proposed reaction mechanism of guaiacol HDO over Ru-HY-60-MI.

3.3 Scope of Ru-HY-60-MI for other lignin representative molecules

Motivated by the successful guaiacol HDO outcomes, other typical lignin representative compounds with α -O-4 bond (diphenyl ether and benzyl phenyl ether), β - β bond (diphenylmethane), side chain (eugenol and isoeugenol), and without methoxy (phenol)

attempted for HDO to yield cycloalkanes. The complete conversion of these compounds and the high yield of corresponding cycloalkanes validate the exceptional performance of Ru-HY-60-MI for different functional surrogates of lignin (Table 4). The diphenyl ether HDO was tested at different conditions to understand the reaction chemistry of C-O-C bond containing compounds over Ru-HY-60-MI. Similar to guaiacol, a high amount of cracking products was observed at low WHSV, high pressure, and temperature (Figure S5). Moreover, methylcyclohexane identification at high temperature suggested the transalkylation reaction. A significant amount of bicyclohexyl confirmed the subsequent alkylation step after the HDO and validated the reaction mechanism given in Scheme 1. Similarly, a high amount of bicyclohexyl (21.6%) as a product of phenol HDO supported the fact that alkylation is a secondary step and suggests that molecules possessing fewer functional groups can readily undergo alkylation during the HDO process. The presence of side chain and C-C bridge bond in propylcyclohexane and dicyclohexylmethane, respectively, indicated that Ru-HY-60-MI can preserve C-C bond in hydrodeoxygenated products at appropriate reaction conditions. While 7% single hydrogenated ring states more severe reaction conditions are required for the complete HDO of diphenylmethane.

Table 4: HDO of lignin model compounds over Ru-HY-60-MI.

406

407

408

409

410

411

412

413

414

415

416

417

418

419

420

421

Substrate	Conversion, wt%	Product select	tivity, wt%	
- OH	>99	72.3%	21.6%	
	>99	84%	13%	
	>99	45%	49%	2%
	>99	2%	91%	7%



Reaction conditions: Catalyst: Ru-HY-60-MI, Pressure - 1 MPa, Temperature - 180 $^{\circ}$ C, WHSV - 1 h⁻¹ All results are with $\pm 2\%$ error.

3.4 HDO of lignin bio-oil over Ru-HY-60-MI

423

424

425

426

427

428

429

430

431

432

433

434

435

436

437

438

439

440

441

442

443

Utilizing the insights gained from the previous experiments, the formulated catalysts were applied to a real system involving lignin bio-oil (20 wt% in guaiacol) as the feedstock, to evaluate its catalytic HDO activity. LBO was prepared using the liquefaction method described in the supplementary materials. The compounds in the pure LBO (prior to guaiacol mixing) were identified and semi-quantified using two-dimensional gas chromatography with time-offlight mass spectrometry (GC×GC-TOF-MS) and flame ionization detector (FID), respectively. Figure S6 displays a contour map of the color-enhanced GC×GC chromatogram, featuring highlighted regions of interest. The color enhancement was achieved by adjusting the color threshold to visualize even the less intense peaks effectively. Within the LBO feed, the depolymerized lignin-derived phenolics can be categorized into two distinct regions: monomeric and dimeric. Typically, the LBO comprises approximately 55% of monomeric and 39% of dimeric lignin-related phenolic compounds. The remaining ~6% is composed of various other components, including paraffins, aromatics, acids, esters, and more. Results indicated pure LBO contained around 24 predominant lignin-derived monomers, mainly phenolics oxygenates, while also includes small amounts of aldehydes, ketones, and esters (Figure S7). Semi-quantitative GC×GC-FID analysis (in area %) with identification of these species was accomplished using GC×GC-TOF-MS with the corresponding NIST library record. These 22 major monomers compounds represent ~94.2% area of total monomers with a \geq 90% MS quality match (Figure S8).

The HDO of diluted LBO in guauaicol was performed at slightly higher temperature (220 °C) as compared to pure lignin representatives (Figure 5). The total hydrodeoxygenated products yield was 84.7wt%. The resulting compounds were cycloalkanes with a tiny amount of alkylbenzenes. Following normalization of guaiacol HDO products (subtracting the guaiacol HDO products), the composition of cyloalkanes comprised 1.4wt% methyl cyclobutane, 4.2 wt% alkylcyclopentanes, 15.3wt% cyclohexane, 62.4wt% alkylcyclohexanes and 11.1wt% dimers. This finding indicates an excellent activity of Ru-HY-60-MI for the HDO of the actual lignin bio-oil in the continuous mode near the moderate reaction conditions.

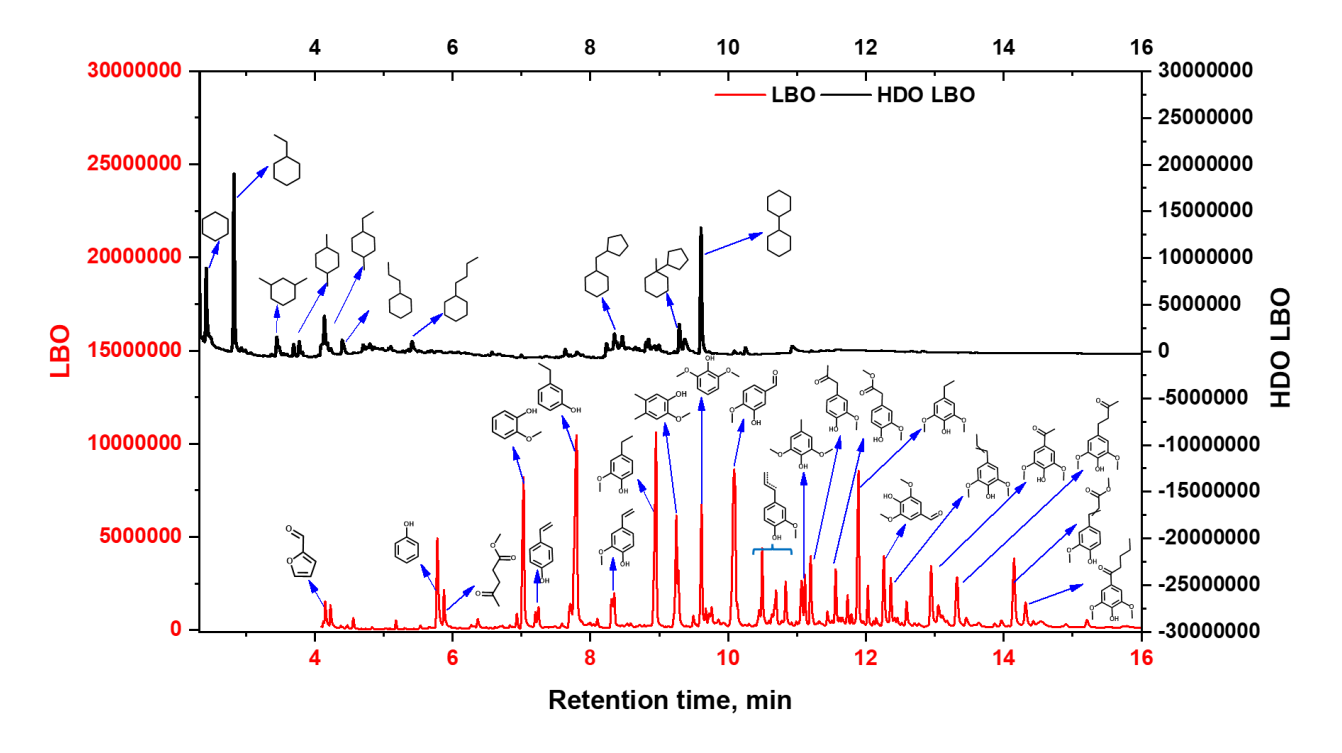


Figure 5: LBO and hydrodeoxygenated LBO product distribution. Reaction conditions: Pressure - 1 MPa, Temperature - 220 °C, WHSV - 1 h^{-1} . Structures verified with GC-MS and GC×GC-TOF-MS.

4. Conclusions

Previous literature reports of guaiacol conversion under moderate conditions (<200 °C and 4 MPa) suffer from low conversion, low selectivity of HDO products, and catalytic site poisoning. The typical incipient wetness impregnation method was modified to prepare a more effective HY zeolite-supported Ru catalyst with better metal dispersion and acid site uniformity

to overcome these challenges. In this study, the development of a Ru-based engineered catalyst has been successfully achieved. Traditional incipient wetness impregnation method has been modified to improve Ru dispersion and reduce the size of Ru metal particles. The addition of acetic acid in modified impregnation method generates C₂H₃O₂⁻ ions, C₂H₃O₂⁻ ions resulted in Ru nanoparticles with a narrow size distribution because of its strong ability to stabilize the primary Ru nanoparticles. The resulting modified catalyst (Ru-HY-60-MI) demonstrated remarkable activity for guaiacol HDO when compared to unmodified catalyst. Proximity of Ru and acid sites in Ru-HY-60-MI simplifies the spillover of guaiacol and intermediates (alkane oxygenates) to and from acid sites at the perimeter of active Ru nanoparticles. Extensive examination of various reaction parameters has validated the possible mechanism of guaiacol HDO over Ru-HY-60-MI, proceeding through a sequence of metal-catalyzed ring hydrogenation of guaiacol to 2-methoxy cyclohexanol, followed by acid-catalyzed demethoxylation and dehydration to cyclohexene and subsequent metal-catalyzed hydrogenation of cyclohexene to cyclohexane. Notably, these HDO reactions were successfully carried out in continuous reactor at moderate conditions (180 °C, 1 h⁻¹ WHSV and 1 MPa hydrogen pressure). Other lignin representatives having different types of bonds (β-β and α -O-4) and lignin bio-oil were successfully converted into cycloalkanes with \geq 84.7 wt% liquid yield. The product composition analysis indicates that hydrodeoxygenation is sensitive to the metal structure, emphasizing the importance of the catalytic configuration in this process. The findings from this research significantly contribute to advancing our knowledge of lignin HDO chemistry under near ambient conditions. Moreover, this new, direct, and efficient continuous lignin HDO process will be optimized so that the maximum impact is achieved with minimal costs and the benefit-to-cost ratio can be improved to produce the lignin-based jet fuel.

Acknowledgement

462

463

464

465

466

467

468

469

470

471

472

473

474

475

476

477

478

479

480

481

482

483

484

We are grateful for support from U.S. Department of Energy DOE-EERE Awards (DE-EE0009257) with the Bioproducts, Science & Engineering Laboratory and Department of Biological Systems Engineering at Washington State University. A portion of the research was performed on a project award from the Environmental Molecular Sciences Laboratory, a DOE Office of Science User Facility sponsored by the Biological and Environmental Research program under Contract No. DE-AC05-76RL01830. Authors sincerely thank David C. Bell (Researcher at Washington State University, Tri-cities) for two-dimensional gas chromatography (GC×GC) analysis of the partial products. RG would like to acknowledge Natural Resources Canada and the government of Canada's interdepartmental program of energy research and development (PERD).

Declaration of Competing Interest

The authors declare that they have no known competing financial interests or personal relationships that could have appeared to influence the work reported in this paper.

Disclaimer

The views and opinions of the authors expressed herein do not necessarily state or reflect those of the United States Government or any agency thereof. Neither the United States Government nor any agency thereof, nor any of their employees, makes any warranty, expressed or implied, or assumes any legal liability or responsibility for the accuracy, completeness, or usefulness of any information, apparatus, product, or process disclosed, or represents that its use would not infringe privately owned rights.

References

- 507 [1] Z. Yang, Z. Xu, M. Feng, J.R. Cort, R. Gieleciak, J. Heyne, B. Yang, Lignin-based jet
- fuel and its blending effect with conventional jet fuel, Fuel, 321 (2022) 124040.
- 509 [2] R. Shen, L. Tao, B. Yang, Techno-economic analysis of jet-fuel production from
- biorefinery waste lignin, Biofuels, Bioproducts and Biorefining, (2018).

- 511 [3] H. Wang, H. Ruan, H. Pei, H. Wang, X. Chen, M.P. Tucker, J.R. Cort, B. Yang, Biomass-
- derived lignin to jet fuel range hydrocarbons via aqueous phase hydrodeoxygenation, Green
- 513 Chemistry, 17 (2015) 5131-5135.
- 514 [4] H. Wang, Y. Pu, A. Ragauskas, B. Yang, From lignin to valuable products-strategies,
- challenges, and prospects, Bioresource technology, 271 (2019) 449-461.
- 516 [5] H. Wang, B. Yang, Q. Zhang, W. Zhu, Catalytic routes for the conversion of
- 517 lignocellulosic biomass to aviation fuel range hydrocarbons, Renewable and Sustainable
- 518 Energy Reviews, 120 (2020) 109612.
- [6] A. Kumar, J. Kumar, T. Bhaskar, Utilization of lignin: A sustainable and eco-friendly
- approach, Journal of the Energy Institute, 93 (2020) 235-271.
- [7] A. Kumar, M. Jindal, S. Maharana, B. Thallada, Lignin Biorefinery: New Horizons in
- 522 Catalytic Hydrodeoxygenation for the Production of Chemicals, Energy & Fuels, 35 (2021)
- 523 16965-16994.
- 524 [8] A.A. Granados Focil, S. Granados Fócil, V.M. Conde Sotelo, R.L. Grimm, F. González
- 525 García, E. Rojas Santiago, C.E. Santolalla Vargas, M.A. Vera Ramirez, J.A. de los Reyes
- Heredia, Development of Bifunctional Hydrodeoxygenation Catalyst Rh-HY for the
- 527 Generation of Biomass-Derived High-Energy-Density Fuels, Energy Technology, 7 (2019)
- 528 1801112.
- 529 [9] K. Agrawal, A. Roldan, N. Kishore, A.J. Logsdail, Hydrodeoxygenation of guaiacol over
- orthorhombic molybdenum carbide: a DFT and microkinetic study, Catalysis Science &
- 531 Technology, 12 (2022) 843-854.
- [10] M. Tan, Y. Yang, Y. Yang, J. Chen, Z. Zhang, G. Fu, J. Lin, S. Wan, S. Wang, Y. Wang,
- 533 Hydrogen spillover assisted by oxygenate molecules over nonreducible oxides, Nature
- 534 Communications, 13 (2022) 1457.
- 535 [11] P. Yan, M.M.-J. Li, E. Kennedy, A. Adesina, G. Zhao, A. Setiawan, M. Stockenhuber,
- The role of acid and metal sites in hydrodeoxygenation of guaiacol over Ni/Beta catalysts,
- 537 Catalysis Science & Technology, 10 (2020) 810-825.
- 538 [12] Z. Tian, X. Liang, R. Li, C. Wang, J. Liu, L. Lei, R. Shu, Y. Chen, Hydrodeoxygenation
- of guaiacol as a model compound of pyrolysis lignin-oil over NiCo bimetallic catalyst:
- 540 Reactivity and kinetic study, Fuel, 308 (2022) 122034.
- 541 [13] F. Broglia, L. Rimoldi, D. Meroni, S. De Vecchi, M. Morbidelli, S. Ardizzone, Guaiacol
- 542 hydrodeoxygenation as a model for lignin upgrading. Role of the support surface features on
- Ni-based alumina-silica catalysts, Fuel, 243 (2019) 501-508.
- [14] E. Roldugina, E. Naranov, A. Maximov, E. Karakhanov, Hydrodeoxygenation of
- 545 guaiacol as a model compound of bio-oil in methanol over mesoporous noble metal catalysts,
- 546 Applied Catalysis A: General, 553 (2018) 24-35.
- 547 [15] A. Kumar, B. Thallada, Hydrodeoxygenation of lignin derived phenolics over a hydrous
- ruthenium oxide based catalyst (s): role of surface water molecules and acidity of the support,
- 549 Sustainable Energy & Fuels, 5 (2021) 3802-3817.
- 550 [16] N.G. Anderson, Practical use of continuous processing in developing and scaling up
- laboratory processes, Organic Process Research & Development, 5 (2001) 613-621.
- 552 [17] P. Yan, J. Mensah, M. Drewery, E. Kennedy, T. Maschmeyer, M. Stockenhuber, Role of
- metal support during ru-catalysed hydrodeoxygenation of biocrude oil, Applied Catalysis B:
- 554 Environmental, 281 (2021) 119470.
- 555 [18] M. López, R. Palacio, A.-S. Mamede, J.J. Fernández, S. Royer, Hydrodeoxygenation of
- 556 guaiacol into cyclohexane over mesoporous silica supported Ni–ZrO2 catalyst, Microporous
- and Mesoporous Materials, 309 (2020) 110452.
- 558 [19] M. Lu, H. Du, B. Wei, J. Zhu, M. Li, Y. Shan, J. Shen, C. Song, Hydrodeoxygenation of
- 559 guaiacol on Ru catalysts: influence of TiO2–ZrO2 composite oxide supports, Industrial &
- 560 Engineering Chemistry Research, 56 (2017) 12070-12079.

- [20] T. Nimmanwudipong, R.C. Runnebaum, K. Brodwater, J. Heelan, D.E. Block, B.C.
- Gates, Design of a high-pressure flow-reactor system for catalytic hydrodeoxygenation:
- 563 guaiacol conversion catalyzed by platinum supported on MgO, Energy & fuels, 28 (2014)
- 564 1090-1096.
- [21] P. Nikulshin, V. Salnikov, A. Varakin, V. Kogan, The use of CoMoS catalysts supported
- on carbon-coated alumina for hydrodeoxygenation of guaiacol and oleic acid, Catalysis
- 567 today, 271 (2016) 45-55.
- 568 [22] H.Y. Zhao, D. Li, P. Bui, S.T. Oyama, Hydrodeoxygenation of guaiacol as model
- compound for pyrolysis oil on transition metal phosphide hydroprocessing catalysts, Applied
- 570 Catalysis A: General, 391 (2011) 305-310.
- 571 [23] J. Sun, A.M. Karim, H. Zhang, L. Kovarik, X.S. Li, A.J. Hensley, J.-S. McEwen, Y.
- Wang, Carbon-supported bimetallic Pd–Fe catalysts for vapor-phase hydrodeoxygenation of
- 573 guaiacol, Journal of catalysis, 306 (2013) 47-57.
- 574 [24] Q. Lai, C. Zhang, J.H. Holles, Hydrodeoxygenation of guaiacol over Ni@ Pd and Ni@
- 575 Pt bimetallic overlayer catalysts, Applied Catalysis A: General, 528 (2016) 1-13.
- 576 [25] R. Olcese, M.M. Bettahar, B. Malaman, J. Ghanbaja, L. Tibavizco, D. Petitjean, A.
- 577 Dufour, Gas-phase hydrodeoxygenation of guaiacol over iron-based catalysts. Effect of gases
- composition, iron load and supports (silica and activated carbon), Applied Catalysis B:
- 579 Environmental, 129 (2013) 528-538.
- 580 [26] D. Gao, C. Schweitzer, H.T. Hwang, A. Varma, Conversion of guaiacol on noble metal
- 581 catalysts: reaction performance and deactivation studies, Industrial & Engineering Chemistry
- 582 Research, 53 (2014) 18658-18667.
- 583 [27] N.T.T. Tran, Y. Uemura, S. Chowdhury, A. Ramli, Vapor-phase hydrodeoxygenation of
- 584 guaiacol on Al-MCM-41 supported Ni and Co catalysts, Applied Catalysis A: General, 512
- 585 (2016) 93-100.
- [28] X. Xu, E. Jiang, Y. Du, B. Li, BTX from the gas-phase hydrodeoxygenation and
- transmethylation of guaiacol at room pressure, Renewable Energy, 96 (2016) 458-468.
- 588 [29] S.T. Thompson, H.H. Lamb, Vapor-phase hydrodeoxygenation of guaiacol over carbon-
- supported Pd, Re and PdRe catalysts, Applied Catalysis A: General, 563 (2018) 105-117.
- 590 [30] Y. Wang, T. He, K. Liu, J. Wu, Y. Fang, From biomass to advanced bio-fuel by catalytic
- 591 pyrolysis/hydro-processing: Hydrodeoxygenation of bio-oil derived from biomass catalytic
- 592 pyrolysis, Bioresource technology, 108 (2012) 280-284.
- 593 [31] J.-S. Moon, E.-G. Kim, Y.-K. Lee, Active sites of Ni2P/SiO2 catalyst for
- 594 hydrodeoxygenation of guaiacol: A joint XAFS and DFT study, Journal of catalysis, 311
- 595 (2014) 144-152.
- 596 [32] Z. He, X. Wang, Highly selective catalytic hydrodeoxygenation of guaiacol to
- 597 cyclohexane over Pt/TiO 2 and NiMo/Al 2 O 3 catalysts, Frontiers of Chemical Science and
- 598 Engineering, 8 (2014) 369-377.
- 599 [33] M. Hellinger, S. Baier, P.M. Mortensen, W. Kleist, A.D. Jensen, J.-D. Grunwaldt,
- 600 Continuous catalytic hydrodeoxygenation of guaiacol over pt/SiO2 and pt/h-mfi-90,
- 601 Catalysts, 5 (2015) 1152-1166.
- 602 [34] T.-S. Nguyen, D. Laurenti, P. Afanasiev, Z. Konuspayeva, L. Piccolo, Titania-supported
- 603 gold-based nanoparticles efficiently catalyze the hydrodeoxygenation of guaiacol, Journal of
- 604 Catalysis, 344 (2016) 136-140.
- 605 [35] H. Fang, J. Zheng, X. Luo, J. Du, A. Roldan, S. Leoni, Y. Yuan, Product tunable
- behavior of carbon nanotubes-supported Ni–Fe catalysts for guaiacol hydrodeoxygenation,
- 607 Applied Catalysis A: General, 529 (2017) 20-31.
- [36] M. Lu, H. Du, B. Wei, J. Zhu, M. Li, Y. Shan, C. Song, Catalytic hydrodeoxygenation of
- guaiacol over palladium catalyst on different titania supports, Energy & Fuels, 31 (2017)
- 610 10858-10865.

- 611 [37] X. Niu, F. Feng, G. Yuan, X. Zhang, Q. Wang, Hollow MFI zeolite supported Pt
- catalysts for highly selective and stable hydrodeoxygenation of guaiacol to cycloalkanes,
- 613 Nanomaterials, 9 (2019) 362.
- 614 [38] H. Fang, W. Chen, S. Li, X. Li, X. Duan, L. Ye, Y. Yuan, Tandem Hydrogenolysis–
- 615 Hydrogenation of Lignin-Derived Oxygenates over Integrated Dual Catalysts with Optimized
- 616 Interoperations, ChemSusChem, 12 (2019) 5199-5206.
- [39] P. Yan, J. Mensah, A. Adesina, E. Kennedy, M. Stockenhuber, Highly-dispersed Ni on
- BEA catalyst prepared by ion-exchange-deposition-precipitation for improved
- 619 hydrodeoxygenation activity, Applied Catalysis B: Environmental, 267 (2020) 118690.
- 620 [40] D.-P. Phan, T.K. Vo, J. Kim, E.Y. Lee, Spray pyrolysis synthesis of bimetallic
- NiMo/Al2O3-TiO2 catalyst for hydrodeoxygenation of guaiacol: Effects of bimetallic
- 622 composition and reduction temperature, Journal of Industrial and Engineering Chemistry, 83
- 623 (2020) 351-358.
- [41] P. Yan, E. Kennedy, M. Stockenhuber, Hydrodeoxygenation of guiacol over ion-
- exchanged ruthenium ZSM-5 and BEA zeolites, Journal of Catalysis, 396 (2021) 157-165.
- 626 [42] C.R. Lee, J.S. Yoon, Y.-W. Suh, J.-W. Choi, J.-M. Ha, D.J. Suh, Y.-K. Park, Catalytic
- roles of metals and supports on hydrodeoxygenation of lignin monomer guaiacol, Catalysis
- 628 Communications, 17 (2012) 54-58.
- 629 [43] L. Wang, J. Zhang, X. Yi, A. Zheng, F. Deng, C. Chen, Y. Ji, F. Liu, X. Meng, F.-S.
- Kiao, Mesoporous ZSM-5 zeolite-supported Ru nanoparticles as highly efficient catalysts for
- upgrading phenolic biomolecules, Acs Catalysis, 5 (2015) 2727-2734.
- 632 [44] P. Yan, E. Kennedy, M. Stockenhuber, Natural zeolite supported Ni catalysts for
- 633 hydrodeoxygenation of anisole, Green Chemistry, 23 (2021) 4673-4684.
- 634 [45] G. Yao, G. Wu, W. Dai, N. Guan, L. Li, Hydrodeoxygenation of lignin-derived phenolic
- compounds over bi-functional Ru/H-Beta under mild conditions, Fuel, 150 (2015) 175-183.
- [46] H. Wang, H. Ben, H. Ruan, L. Zhang, Y. Pu, M. Feng, A.J. Ragauskas, B. Yang, Effects
- of lignin structure on hydrodeoxygenation reactivity of pine wood lignin to valuable
- chemicals, ACS Sustainable Chemistry & Engineering, 5 (2017) 1824-1830.
- 639 [47] H. Wang, H. Wang, E. Kuhn, M.P. Tucker, B. Yang, Production of Jet Fuel-Range
- 640 Hydrocarbons from Hydrodeoxygenation of Lignin over Super Lewis Acid Combined with
- 641 Metal Catalysts, ChemSusChem, 11 (2018) 285-291.
- [48] H. Wang, L. Zhang, T. Deng, H. Ruan, X. Hou, J.R. Cort, B. Yang, ZnCl2 induced
- catalytic conversion of softwood lignin to aromatics and hydrocarbons, Green Chemistry, 18
- 644 (2016) 2802-2810.
- [49] D.D. Laskar, M.P. Tucker, X. Chen, G.L. Helms, B. Yang, Noble-metal catalyzed
- 646 hydrodeoxygenation of biomass-derived lignin to aromatic hydrocarbons, Green Chemistry,
- 647 16 (2014) 897-910.
- [50] D.C. Elliott, H. Wang, R. French, S. Deutch, K. Iisa, Hydrocarbon Liquid Production
- 649 from Biomass via Hot-Vapor-Filtered Fast Pyrolysis and Catalytic Hydroprocessing of the
- 650 Bio-oil, Energy & Fuels, 28 (2014) 5909-5917.
- [51] A. Kumar, A. Kumar, B. Biswas, J. Kumar, S.R. Yenumala, T. Bhaskar,
- 652 Hydrodeoxygenation of m-Cresol over Ru based catalysts: Influence of catalyst support on
- 653 m-Cresol conversion and methylcyclohexane selectivity, Renewable Energy, 151 (2020) 687-
- 654 697.
- 655 [52] H. Ruan, Z. Xu, A. Kumar, M. Feng, A.S. Lipton, E.D. Walter, R. Gieleciak, H.P.
- Paudel, Y. Duan, B. Yang, Elucidating the Reaction Pathways of Veratrylglycero-β-Guaiacyl
- Ether Degradation over Metal-Free Solid Acid Catalyst with Hydrogen, ChemSusChem, 16
- 658 (2023) e202202001.

- 659 [53] H. Zou, J. Dai, J. Suo, R. Ettelaie, Y. Li, N. Xue, R. Wang, H. Yang, Dual metal
- 660 nanoparticles within multicompartmentalized mesoporous organosilicas for efficient
- sequential hydrogenation, Nature Communications, 12 (2021) 4968.
- [54] D.K. Mishra, A.A. Dabbawala, J.-S. Hwang, Ruthenium nanoparticles supported on
- zeolite Y as an efficient catalyst for selective hydrogenation of xylose to xylitol, Journal of
- Molecular Catalysis A: Chemical, 376 (2013) 63-70.
- [55] N.S. Gould, B. Xu, Quantification of acid site densities on zeolites in the presence of
- solvents via determination of extinction coefficients of adsorbed pyridine, Journal of
- 667 catalysis, 358 (2018) 80-88.
- [56] P. Gogoi, A.S. Nagpure, P. Kandasamy, C.V.V. Satyanarayana, T. Raja, Insights into the
- catalytic activity of Ru/NaY catalysts for efficient H2 production through aqueous phase
- reforming, Sustainable Energy & Fuels, 4 (2020) 678-690.
- [57] D.R.S. Pedrolo, V.V. Ordomsky, M. Schwaab, N.R. Marcilio, A.Y. Khodakov, Design
- of ruthenium-zeolite nanocomposites for enhanced hydrocarbon synthesis from syngas,
- 673 Journal of Materials Science, 56 (2021) 18019-18030.
- [58] A.M. Pourrahimi, D. Liu, L.K.H. Pallon, R.L. Andersson, A. Martínez Abad, J.M.
- Lagarón, M.S. Hedenqvist, V. Ström, U.W. Gedde, R.T. Olsson, Water-based synthesis and
- 676 cleaning methods for high purity ZnO nanoparticles comparing acetate, chloride, sulphate
- and nitrate zinc salt precursors, RSC Adv., 4 (2014) 35568-35577.
- 678 [59] A. Redjel, A.-G. Boudjahem, M. Bettahar, Effect of palladium precursor and preparation
- 679 method on the catalytic performance of Pd/SiO2 catalysts for benzene hydrogenation,
- Particulate Science and Technology, 36 (2018) 710-715.
- 681 [60] X. Wu, Z. Wang, D. Zhang, Y. Qin, M. Wang, Y. Han, T. Zhan, B. Yang, S. Li, J. Lai,
- L. Wang, Solvent-free microwave synthesis of ultra-small Ru-Mo2C@CNT with strong
- 683 metal-support interaction for industrial hydrogen evolution, Nature Communications, 12
- 684 (2021) 4018.
- [61] G. Xiang, X. Shi, Y. Wu, J. Zhuang, X. Wang, Size effects in Atomic-Level Epitaxial
- Redistribution Process of RuO2 over TiO2, Scientific Reports, 2 (2012) 801.
- 687 [62] S. Wang, K. Zhang, H. Li, L.-P. Xiao, G. Song, Selective hydrogenolysis of catechyl
- 688 lignin into propenylcatechol over an atomically dispersed ruthenium catalyst, Nature
- 689 Communications, 12 (2021) 416.
- 690 [63] Y. Shao, Q. Xia, L. Dong, X. Liu, X. Han, S.F. Parker, Y. Cheng, L.L. Daemen, A.J.
- Ramirez-Cuesta, S. Yang, Y. Wang, Selective production of arenes via direct lignin
- 692 upgrading over a niobium-based catalyst, Nature Communications, 8 (2017) 16104.
- 693 [64] J.E. Peters, J.R. Carpenter, D.C. Dayton, Anisole and Guaiacol Hydrodeoxygenation
- Reaction Pathways over Selected Catalysts, Energy & Fuels, 29 (2015) 909-916.
- 695 [65] K.M. Bratlie, H. Lee, K. Komvopoulos, P. Yang, G.A. Somorjai, Platinum nanoparticle
- shape effects on benzene hydrogenation selectivity, Nano letters, 7 (2007) 3097-3101.
- 697 [66] P.M. Mortensen, J.-D. Grunwaldt, P.A. Jensen, A.D. Jensen, Influence on nickel particle
- size on the hydrodeoxygenation of phenol over Ni/SiO2, Catalysis Today, 259 (2016) 277-
- 699 284.
- 700 [67] N. Duong, Q. Tan, D.E. Resasco, Controlling phenolic hydrodeoxygenation by tailoring
- 701 metal—O bond strength via specific catalyst metal type and particle size selection, Comptes
- 702 Rendus Chimie, 21 (2018) 155-163.
- 703 [68] A.R. De la Osa, A. Romero, F. Dorado, J.L. Valverde, P. Sánchez, Influence of Cobalt
- 704 Precursor on Efficient Production of Commercial Fuels over FTS Co/SiC Catalyst, Catalysts,
- 705 6 (2016) 98.
- 706 [69] V.V. Pushkarev, K. An, S. Alayoglu, S.K. Beaumont, G.A. Somorjai, Hydrogenation of
- benzene and toluene over size controlled Pt/SBA-15 catalysts: Elucidation of the Pt particle
- size effect on reaction kinetics, Journal of catalysis, 292 (2012) 64-72.

- 709 [70] T.O. Omotoso, B. Baek, L.C. Grabow, S.P. Crossley, Experimental and first-principles
- evidence for interfacial activity of Ru/TiO2 for the direct conversion of m-cresol to toluene,
- 711 ChemCatChem, 9 (2017) 2642-2651.
- 712 [71] T.W. van Deelen, C. Hernández Mejía, K.P. de Jong, Control of metal-support
- interactions in heterogeneous catalysts to enhance activity and selectivity, Nature Catalysis, 2
- 714 (2019) 955-970.
- 715 [72] N.K.G. Silva, R.A.R. Ferreira, R.M. Ribas, R.S. Monteiro, M.A.S. Barrozo, R.R. Soares,
- Gas-phase hydrodeoxygenation (HDO) of guaiacol over Pt/Al2O3 catalyst promoted by
- 717 Nb2O5, Fuel, 287 (2021) 119509.
- 718 [73] P. Yan, G. Bryant, M.M.-J. Li, J. Mensah, E. Kennedy, M. Stockenhuber, Shape
- selectivity of zeolite catalysts for the hydrodeoxygenation of biocrude oil and its model
- compounds, Microporous and Mesoporous Materials, 309 (2020) 110561.
- 721 [74] R. Kallury, T.T. Tidwell, D.G.B. Boocock, D.H.L. Chow, High temperature catalytic
- hydrogenolysis and alkylation of anisole and phenol, Canadian journal of chemistry, 62
- 723 (1984) 2540-2545.
- 724 [75] L. Nie, B. Peng, X. Zhu, Vapor-Phase Hydrodeoxygenation of Guaiacol to Aromatics
- over Pt/HBeta: Identification of the Role of Acid Sites and Metal Sites on the Reaction
- 726 Pathway, ChemCatChem, 10 (2018) 1064-1074.
- 727 [76] A.V. Vutolkina, I.G. Baigildin, A.P. Glotov, A.A. Pimerzin, A.V. Akopyan, A.L.
- Maximov, E.A. Karakhanov, Hydrodeoxygenation of guaiacol via in situ H2 generated
- 729 through a water gas shift reaction over dispersed NiMoS catalysts from oil-soluble
- 730 precursors: Tuning the selectivity towards cyclohexene, Applied Catalysis B: Environmental,
- 731 312 (2022) 121403.
- 732 [77] P. Castaño, J.M. Arandes, M. Olazar, J. Bilbao, B. Pawelec, U. Sedrán, Effect of
- hydrogen on the cracking mechanisms of cycloalkanes over zeolites, Catalysis Today, 150
- 734 (2010) 363-367.

- 735 [78] O.V. Potapenko, M.S. Khudyakov, E.O. Altynkovich, K.S. Plekhova, T.P. Sorokina,
- 736 V.P. Doronin, Catalytic cracking of cyclohexane and 1-hexene mixtures on mono-, bi-, and
- tri-zeolite catalysts, Kinetics and Catalysis, 60 (2019) 74-86.
- 738 [79] G. Nie, Y. Dai, Y. Liu, J. Xie, S. Gong, N. Afzal, X. Zhang, L. Pan, J.-J. Zou, High yield
- one-pot synthesis of high density and low freezing point jet-fuel-ranged blending from bio-
- derived phenol and cyclopentanol, Chemical Engineering Science, 207 (2019) 441-447.